ACS APPLIED ENERGY MATERIALS

www.acsaem.org Article

Effective Synthesis Procedure Based on Microwave Heating of the PdCo Aerogel Electrocatalyst for Its Use in Microfluidic Devices

A. Martínez-Lázaro, A. P. Mendoza-Camargo, M. H. Rodriguez-Barajas, F. I. Espinosa-Lagunes, Y. Salazar-Lara, A. Herrera-Gomez, O. Cortazar-Martínez, N. Rey-Raap, J. Ledesma-García,* A. Arenillas,* and L. G. Arriaga

Cite This: *ACS Appl. Energy Mater.* 2023, 6, 6410−6418 Read Online

ACCESS | Metrics & More | Article Recommendations | Supporting Information

ABSTRACT: Unsupported PdCo aerogels were successfully synthesized by means of microwave heating. The use of this heating methodology provides some advantages compared to conventional heating in terms of saving synthesis time and improved physicochemical properties (i.e., greater surface area and mesoporosity). The combination of palladium with cobalt reduces the dependence of the noble metal and increases the electrocatalytic performance in the ethanol oxidation reaction due to a higher percentage of Pd^0 in the PdCo aerogel, confirmed using the X-ray photoelectron spectroscopy (XPS) technique. For the application in energy conversion electrochemical systems, the catalytic activity of aerogels was evaluated in a microfluidic fuel cell that uses ethanol as fuel, where the PdCo aerogel synthesized by microwave heating exhibited great performance with 330 mA cm^{-2} current density, tripling the value of the palladium-based aerogel.

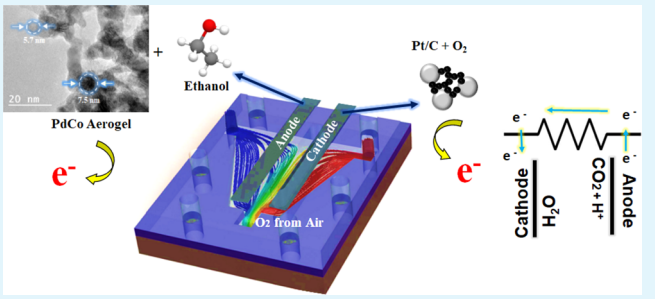

KEYWORDS: *microwave heating, bimetallic aerogel, microfluidic fuel cell, high-surface electrocatalyst, ethanol oxidation reaction*

1. INTRODUCTION

In the last years, microfluidic fuel cells (MFCs) have shown significant advances due to their relevance and versatility in many microscale applications as portable devices.[1] MFCs avoid the use of conventional polymeric membranes since they are based on laminar flows with ion exchange at the interface between them.[2] Various fluids have been evaluated in a series of devices such as blood or sweat and some fuels such as hydrogen or hydrocarbons.[3] To date, different MFC configurations have been reported, where different factors affect the performance of the device, the main one being the catalyst used at both the anode and cathode. Hence, the continuous improvement of catalysts used for fuel cells and other electrochemical devices and systems is one of the current challenges to ensure the performance of these technologies.[4] Despite the fact that countless innovative materials have currently been developed for several fuel oxidation reactions, noble metal-based catalysts such as Pt, Ag, and Pd still play a predominant role because of their superior catalytic activity, resistance to corrosion, and high electrochemical stability. Therefore, these precious metals guarantee a good performance of MFCs. However, the scarcity and high cost continue to be an impediment for massive use in these devices. Aerogels have emerged as an interesting proposal to solve the excessive use of noble metals thanks to their high porosity and surface area.[5,6] Aerogels allow the use of very small amounts of the catalyst while maintaining their catalytic effectiveness.[7] The advantages of their morphology and ultralow density give aerogels a relevant role in nanotechnology and heterogeneous catalysis.[8,9] Several aerogels have been evaluated toward electrochemical oxidation reactions such as Pd,[10,11] bimetallic materials such as Ag or Cu,[7] noble metal aerogels supported on carbon-based materials,[12] and Pt aerogels.[7,8,13]

On the other hand, there are several investigations where the oxidation processes are carried out using different types of fuel as formic acid,[14−16] glycerol,[17] or ethanol.[18] The proposal toward improving aerogels as catalysts is functionalizing them with transition metals abundant in the earth such as Co, Ni, and Mn. The incorporation of transition metal atoms in the structure of a noble metal aerogel could be a great step toward the continuous improvement of this innovative material. The main advantage provided by the transition metals will be the increase of the catalytic activity and the low cost of the material due to their abundance in nature.[19] The optimal composition between noble and transition metals will benefit the catalytic

Received: January 23, 2023
Accepted: May 26, 2023
Published: June 9, 2023

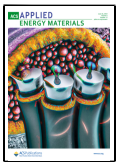

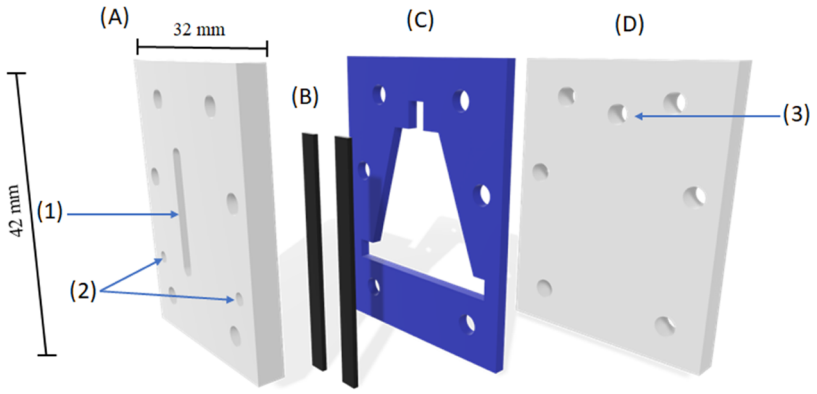

Figure 1. Microfluidic fuel cell (MFC)-type "Y" configuration. (A) Top cover, (B) carbon paper electrodes, (C) silastic gaskets, and (D) lower cover.

performance, chemical stability, and corrosion resistance, which are characteristics of noble metals.[20,21]

In this work, a bimetallic aerogel is synthesized by incorporation of a transition metal (cobalt) in the noble metal structure (palladium) by means of a novel process based on microwave heating. The effect of the heating technology (i.e., microwave vs conventional heating) is also analyzed in terms of physicochemical properties and electrocatalytic performance of the aerogel. As a practical application, the PdCo aerogel has also been evaluated in a microfluidic fuel cell that works with ethanol as fuel.

2. EXPERIMENTAL SECTION

2.1. Aerogel Synthesis. The synthesis of Pd−Co aerogels was carried out by adding 10 mL of $PdCl_2$ (2 mg/mL, 99% Sigma-Aldrich ReagentPlus) to a solution of sodium carbonate (≥99.5%, J. T. Baker) and glyoxylic acid monohydrate (98% Sigma-Aldrich) (ratio 6:1) in 40 mL of deionized DI water. The mixture was heated at 68 °C for 2 h for the nucleation reaction. The gelation process elapsed for 7 h at 45 °C. Two different PdCo samples were prepared: The first one, PdCo-MW, consisted of PdCo obtained by microwave heating (MW) in two steps (i.e., nucleation and gelation process). Meanwhile, the second material PdCo-OV was synthesized with the same procedure as the first one, except for using conventional heating in an oven (OV) for the same time (2 h at 68 °C for nucleation and 7 h at 45 °C for gelation). For control experiments, a palladium aerogel, Pd-MW, was obtained by microwave heating at the same conditions of PdCo-MW. Samples from the wet gels were washed several times with DI water and ethanol. Three samples were cooled to room temperature for washing before drying. The drying process was performed with a residual volume of 3 mL of DI water. The mixture was then frozen with liquid N_2, and the solvent was eliminated by lyophilization (HyperCOOL, model: HC3110) at −110 °C for 1 day (Figure S1).

2.2. Physicochemical Characterization. The crystal structures were characterized by X-ray diffraction (XRD; D8-advance diffractometer Bruker) equipped with a Cu Kα X-ray source (λ = 0.1541 nm, 40 kV, 40 mA,), using a step size of 0.02° 2θ and a scan step time of 5 s. The morphology of the aerogel samples was characterized using a JEOL JEM-2100F high-resolution transmission electron microscope (HR-TEM) with spherical aberration correction. The specific surface area and the pore size distribution were estimated by nitrogen adsorption−desorption isotherms at −196 °C (Micromeritics ASAP 2020), after overnight outgassing at 120 °C. The electronic structure of elements was measured by X-ray photoelectron spectroscopy (XPS; K-Alpha+ spectrometer equipped with the Avantage Data System from Thermo Scientific).

2.3. Ethanol Oxidation Reaction Evaluation. Electrochemical performance toward the ethanol oxidation reaction (EOR) for PdCo and Pd aerogels was carried out in a Biologic VMP3 potentiostat/galvanostat using a conventional three-electrode electrochemical cell in acid media at 20 mV s^{-1} scan rate. A glassy carbon electrode (3 mm diameter) was used as the working electrode, with a Ag/AgCl electrode and a Pt wire as reference and counter electrodes, respectively. The electrocatalyst ink was prepared using each aerogel sample in a mixture of DI water (500 μL) + Nafion (5%, 50 μL) per milligram of the catalyst. The ink was sonicated for 1 hour, and then, 10 μL was deposited over the electrode surface. The electrolyte was bubbled with N_2 for 30 minutes before the electrochemical measurements. Electrochemical profiles were obtained using the cyclic voltammetry technique (CV); all experiments were performed in 1 M KOH in the absence or presence of 0.5 M ethanol within a potential range between −0.1 and 1.8 V vs RHE, where the faradaic processes were visible in a mass current, normalized by mg of the catalyst.

2.4. Microfluidic Fuel Cell Configuration. The description of the microfluidic fuel cell (MFC) type "Y" configuration has been previously reported by our group.[22] Briefly, according to Figure 1, the top cover made of acrylic (A) had 19.5 mm height with a slot by air-breathing arrangement (1) and fluid injection area (2). (B) A pair of carbon paper electrodes (41 mm height and 3 mm width) is placed. (C) It corresponds to a Silastic membrane with a geometric adaptation that favors the formation of a microfluidic exchange zone. (D) It is a lower cover made with acrylic, which contains a groove to vent fluids (3). The air-breathing cathodic compartment was equipped with a commercial catalyst based on Pt/C (10 wt %, Alfa Aesar) and 0.5 M H_2SO_4 previously bubbled with O_2 for 30 minutes, as a catholyte. The flux rate was 200 μL min^{-1} in both MFC compartments. The linear sweep voltammetry (LSV) technique was used to obtain curves from open-circuit voltage (OCV) until 0 V to observe the mass current obtained. The chronoamperometric test was carried out at 1.1 V for 3 days in order to evaluate the catalyst stability.

3. RESULTS

3.1. Physicochemical Characterization. XRD patterns of the synthesized aerogels are shown in Figure 2. In addition, the crystallite size was calculated using the Scherrer equation

$$d_{111} = \frac{K\lambda}{\beta_{111}\cos\theta} \quad (1)$$

XRD patterns for PdCo-MW and Pd-MW aerogels were observed with four major diffraction peaks appearing at the 2Θ values. The peak with the highest intensity was taken for the calculation of crystallite size. In the Pd-MW aerogel, the peaks were 40.1, 46.5, 68.1, and 82.1°, which are ascribed to the (111), (200), (220), and (311) reflection planes of Pd (JCPDS #46-1043), respectively. These peaks agree with a face-centered cubic (FCC) crystal structure. The resulting aerogels revealed characteristic Pd peaks and a shift in position (111) to

https://doi.org/10.1021/acsaem.3c00173
ACS Appl. Energy Mater. 2023, 6, 6410−6418

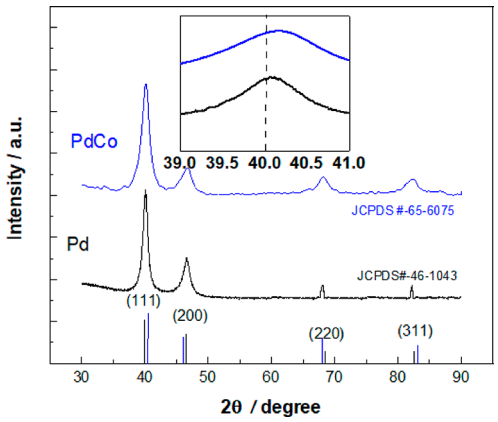

Figure 2. XRD patterns for PdCo-MW and Pd-MW samples.

the left, suggesting the presence of PdCo alloys as shown in Figure 2. The PdCo aerogel presents peaks in 2Θ, which were 40.4, 46.2, 68.1, and 81.8°, compared with the reference JCPDS #65-6075 corresponding to PdCo, which has a peak with high intensity in 2Θ with a value of 41.7° corresponding to the reflection plane (111), being further away from the one obtained and coinciding even more with the JCPDS #46-1043 of Pd.

The crystallite sizes obtained using the 2Θ values of 40.1 and 40.35° with the Scherrer equation (eq 1) were 9.46 and 3.70 nm for Pd-MW and PdCo-MW, respectively. There is a great difference between materials, detecting a notable decrease of crystallite size for PdCo-MW compared to that obtained for the Pd aerogel.

HR-TEM was performed to characterize the morphology and structure of the synthesized aerogels. The analysis reveals interconnected clusters at nanometric size, not independent nanoparticles, which are related to the typical structure seen in all sol−gel materials (Figure 3). TEM images at different magnifications show chains of particles defining pores of different sizes between them, typically a characteristic for aerogels. The sample PdCo-MW shows particle sizes between 5.7 and 7.5 nm, similar to those of the sample PdCo-OV (between 5.6 and 7 nm). It seems that transition metal incorporation allows obtaining smaller particles than the ones formed in Pd-MW, where particles up to 8 nm can be observed. These particle sizes are going to be important for the porosity and specific surface area developed in these aerogels, which in turn are relevant for the further superficial reactions that could take place in any application, as will be discussed later.

At higher magnification, it can be seen that the interplanar distances are wider for cobalt-containing catalysts, which can be attributed to the presence of the alloy between the two metals used in the synthesis.[23−25] The interplanar distance for Pd-MW is 0.22 nm, while the incorporation of transition metals increases this value to 0.24 and 0.255 for PdCo-OV and PdCo-MW, respectively. This may be interpreted as cobalt and palladium crystals coexisting in the chemical structure of the nanoparticles.[25−28] The slight differences between PdCo-MW and PdCo-OV could be attributed to different chemical compositions due to the different heating processes employed during the synthesis process.

In addition, the N_2 adsorption/desorption isotherms presented in Figure 4 clearly show that the materials present a mesoporous structure: (i) there is an increasing N_2 adsorption volume at intermediate relative pressures and (ii) there is a hysteresis loop in the desorption isotherm. This mesoporous structure can only be obtained if the materials are aerogels; otherwise, this structure would not be developed. Furthermore, in the case of nanoparticles, the N_2 adsorption isotherms usually exhibit a sharp increase in the adsorbed volume near the saturation point (P/P_0 = 1) due to interparticular condensation, but this is not the case as the adsorption is gradual with the relative pressure. Therefore, it is clearly demonstrated that the materials presented in this article are indeed bimetallic aerogels. The surface area of the samples was determined using the BET equation, obtaining values of 63, 58, and 50 $m^2\ g^{-1}$ for PdCo-MW, PdCo-OV, and Pd-MW, respectively.

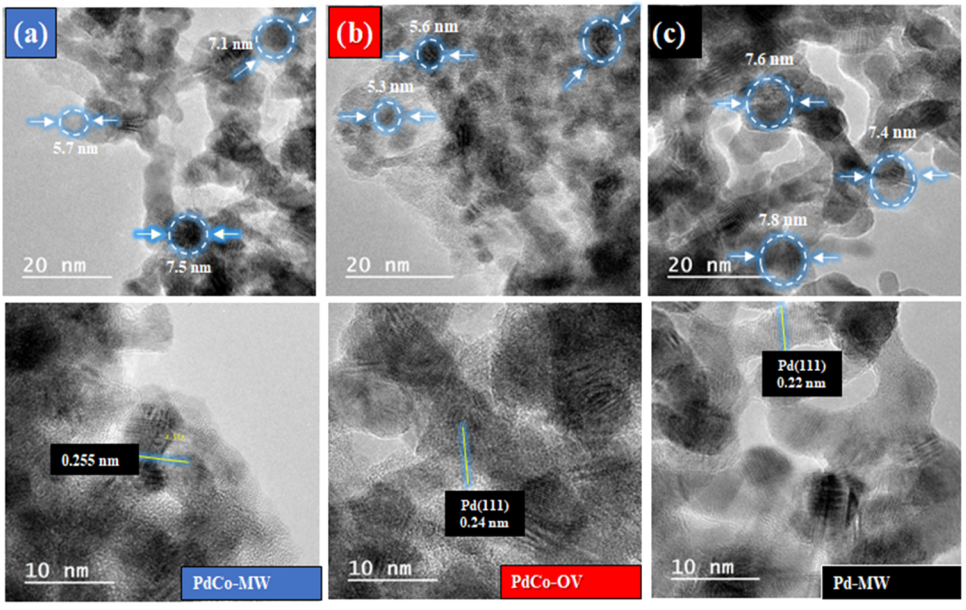

Figure 3. HR-TEM images of aerogel samples. (a) PdCo-MW; (b) PdCo-OV; and (c) Pd-MW.

https://doi.org/10.1021/acsaem.3c00173
ACS Appl. Energy Mater. 2023, 6, 6410−6418

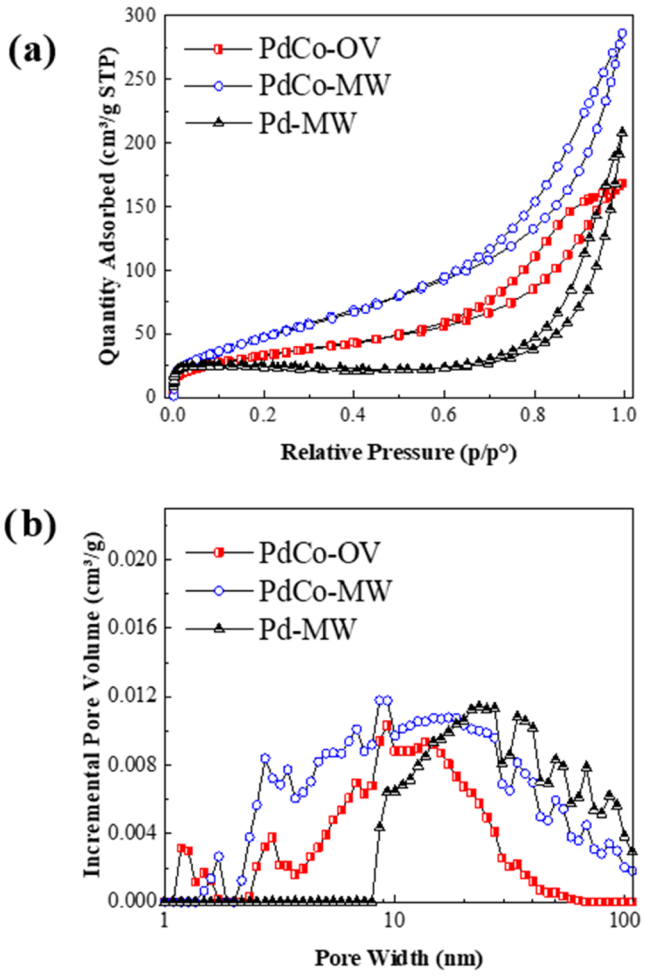

Figure 4. (a) BET analysis of aerogels. (b) Pore size distribution in aerogel samples.

Using the X-ray photoelectron spectroscopy (XPS) technique, the analysis of PdCo aerogels was performed in all samples to know the chemical composition and oxidation states (Figure 5). The broad spectrum of the sample, as shown in Figure 5a, indicates the presence of C, Pd, Co, and O peaks of impurities such as Na and Si, which are typical of the synthesis of the study material. The spectrum of Pd 2p is observed in Figure 5b, having binding energies for Pd $3d_{3/2}$ and Pd $3d_{5/2}$, corresponding to the peaks of 340.7 and 335.55 eV, respectively.

The deconvoluted spectrum shows the energy band values at peaks with 336.43 and 341.76 eV at Pd^{2+}. In contrast, those located at 335.15 and 340.5 eV refer to Pd^0, which is attributed to an oxidation state,[27−29] constituting the Pd/PdO. However, when comparing the synthesized aerogels, a higher concentration of Pd^{2+} is shown for the PdCo-OV sample than for the PdCo-MW sample, so the heating process of the PdCo-MW aerogel presents more stability by containing a higher concentration of Pd^0.

High-resolution Co 2p scanning is presented in Figure 5c, where the spectra of Co 2p exhibit two prominent peaks with binding energies of 780 and 796 eV corresponding to Co $2p_{3/2}$ and Co $2p_{1/2}$, respectively. The difference between the peaks of Co 2p is due to the splitting energy of the spin−orbit. The oxidation state of cobalt ions was determined from the high-resolution spectra of Co 2p by the Lorentzian−Gaussian adjustment method, where the adjusted peaks correspond to the binding energy values, giving the peaks of 780.5 and 795.4 eV corresponding to Co^{2+}, and those located at 782.2 and 797.7 eV refer to Co^{3+}, with a margin of error of the binding energies reported for the structure for Co_3O_4;[30−3230−32] however, by comparison of the samples, there is no difference in the signals of the peaks. Hence, it has the presence of the CoPd alloy on the surface, having two spectra in their oxidation state. The quantitative evaluation of each peak was obtained by dividing the area of the peak, which was calculated from the cross sections and the mean depth of the escape electrons. XPS data were interpreted using Avantage Thermo software with angular resolution (ARXPS), where molar proportions were obtained as Co0.72Pd0.1, in addition to calculating the percentage of the relative weight of the sample, where also, 18% C was found,[24,28] where there is a higher percentage of Pd^{2+} with 40.3% than Pd^0 at 30.5% for the PdCo-OV sample.[33]

The 3d spectra of Pd collected during the pretreatment processes showed that on the surface of the aerogels, the Pd was partially oxidized, as expected.[34] However, the Co remained oxidized, with few perceptible changes in the region of the Co 2p spectrum. In comparison, for the PdCo-MW sample, there is a higher concentration of Pd^0 at 35.8%. This shows that PdCo aerogels can oxidize during the carbonization process in the heating techniques presented, resulting in greater oxidation of the Pd-MW sample. In contrast, the PdCo-MW sample presents the stability of the material by not undergoing total oxidation, which is consistent with the results of TEM and electrochemical tests presenting a better response in microwave heating of the sample PdCo-MW.[35]

3.2. Electrochemical Performance. Aerogel samples were evaluated by cyclic voltammetry (CV) to determine their electrocatalytic activity toward the ethanol oxidation reaction (EOR) in potential ranges between −0.1 and 1.8 V vs RHE (all potential values were normalized vs RHE). Electrochemical profiles in the absence of ethanol were obtained in 1 M KOH at ambient conditions and 20 mV s^{-1} scan rate (Figure 6). The resulting voltammograms show the peaks attributed to Pd activity: (i) the hydrogen desorption in the range of 0.3−0.5V, (ii) hydrogen adsorption at 0.35 V, (iii) Pd(II) oxide reduction at 0.75 V, and (iv) Pd(II) oxide formation at 1.38 V. However, the samples obtained in this work also contain Co; therefore, there are other peaks that may be attributed to the oxidation (v) and reduction (vi) of Co metal species (Figure 6a). For the PdCo aerogels, oxidation and reduction processes are observed between 0.9 and 1.55 V vs RHE.

The use of microwave heating during the synthesis steps clearly improves the electrochemical activity of PdCo-MW. The lower particle size detected by TEM and the higher content of the Pd^0 present in the PdCo-MW evaluated by XPS show clearly that this synthesis procedure has a great impact on the electrochemical performance of the aerogels compared to that obtained using a convectional heating process as in the case of PdCo-OV.

The evaluation of the EOR was carried out in the same range of potential as the CV tests, where it can be seen that the mass current for the PdCo-MW aerogel was clearly superior to that obtained when PdCo-OV was used (Figure 6b). Furthermore, compared with the sample that only contains Pd, the current density value obtained with the material based on PdCo-MW was almost 3 times greater than that obtained

https://doi.org/10.1021/acsaem.3c00173
ACS Appl. Energy Mater. 2023, 6, 6410−6418

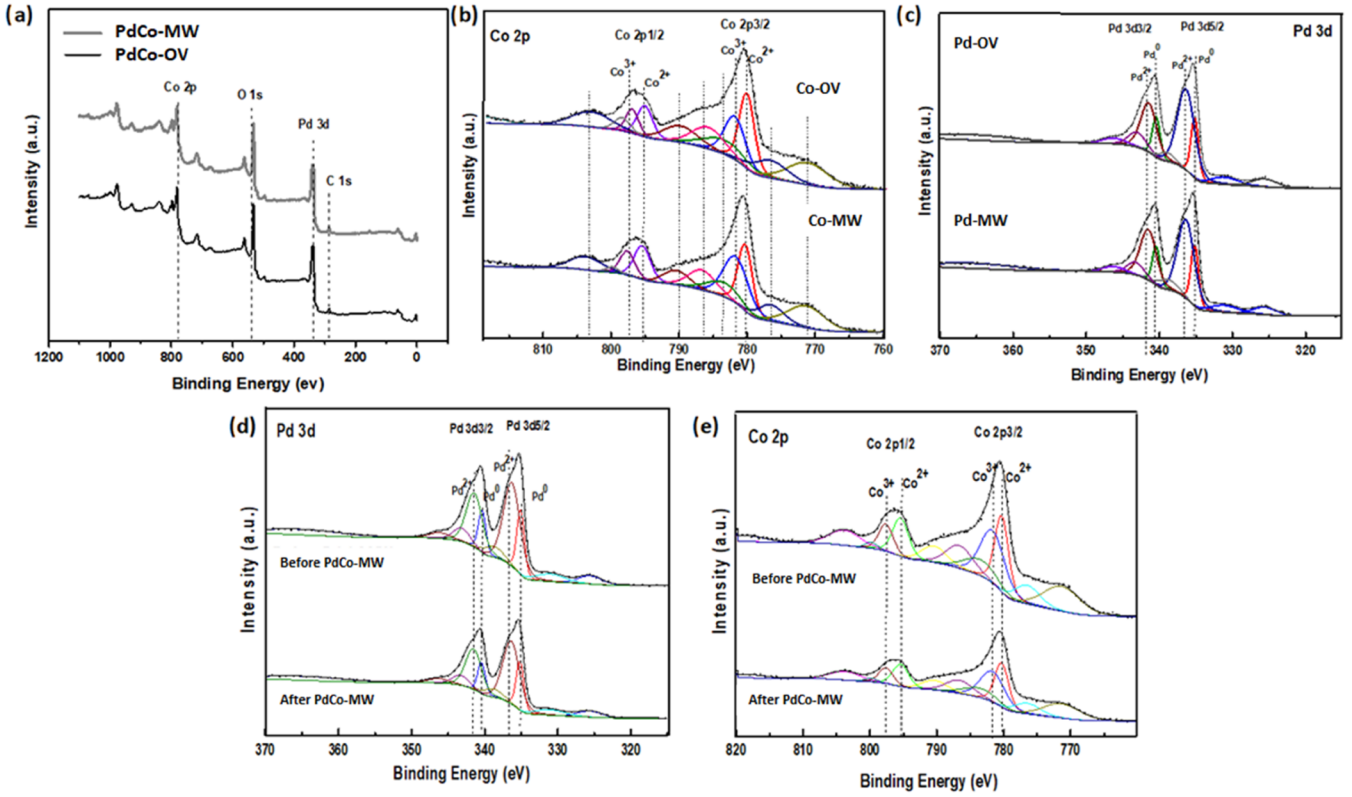

Figure 5. XPS analysis for Pd and Co species in PdCo aerogels. (a) High-resolution general spectra of PdCo aerogels. (b) Evaluation of spectra in the Co 2p region. (c) Evaluation of spectra in the Pd 3d region. (d) Comparison of spectra in the Pd 3d region before and after the stability test of the PdCo-MW aerogel. (e) Comparison of spectra in the Co 2p region before and after the stability test of the PdCo-MW aerogel.

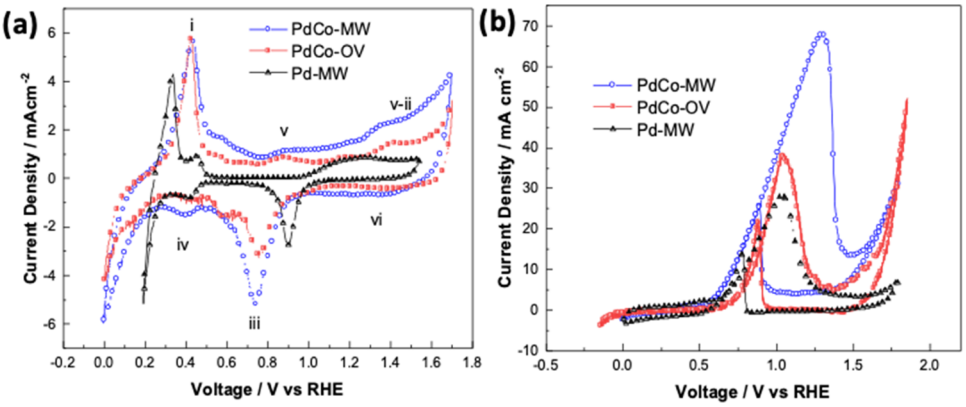

Figure 6. Comparative voltammograms of PdCo-MW, PdCo-OV, and Pd-MW in 1 M KOH (a) in the absence of ethanol and (b) in the presence of 0.5 M ethanol.

Table 1. Comparison of Electrocatalysts Used for the EOR in Alkaline Media Reported to Date

Sample	Ethanol Concentration	Electrolyte	Maximum ell Voltage	Maximum Current Density (mA cm^{-2})	Reference
Pd/C	1 M	1 M KOH	0.78 V vs RHE	30	36
Ni@Pd-Ni NAs	0.5 M	1 M KOH	−0.25 V	50	37
NiPd	1 M	1 M NaOH	0.82 V vs RHE	4.1	38
Au@Pd/C	1 M	1 M KOH	−0.19 V vs MMO	10.5	39
NCNT-Pd	0.1 M	1 M KOH	−0.39 V vs Ag/AgCl	10.30	40
$cPd(DBA)_2$	0.5 M Gly/KOH	1 M KOH	0.08 V vs NHE	16	41
Pd-MW	1 M	1 M KOH	1.03 V vs RHE	28	this work
PdCo-OV	1 M	1 M KOH	1.05 V vs RHE	37	this work
PdCo-MW	1 M	1 M KOH	1.28 V vs RHE	70	this work

https://doi.org/10.1021/acsaem.3c00173
ACS Appl. Energy Mater. 2023, 6, 6410−6418

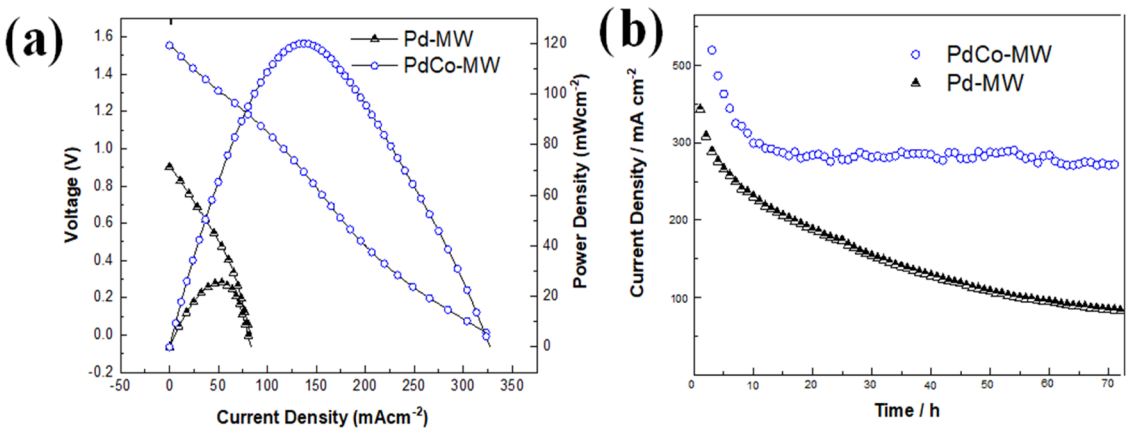

Figure 7. (a) Polarization and power density curves of MFC using 1 M ethanol as fuel and O_2 as an oxidant and Pd-based aerogels as anodic electrocatalysts. (b) Stability test performance of the MFC using PdCo-MW and Pd-MW aerogels.

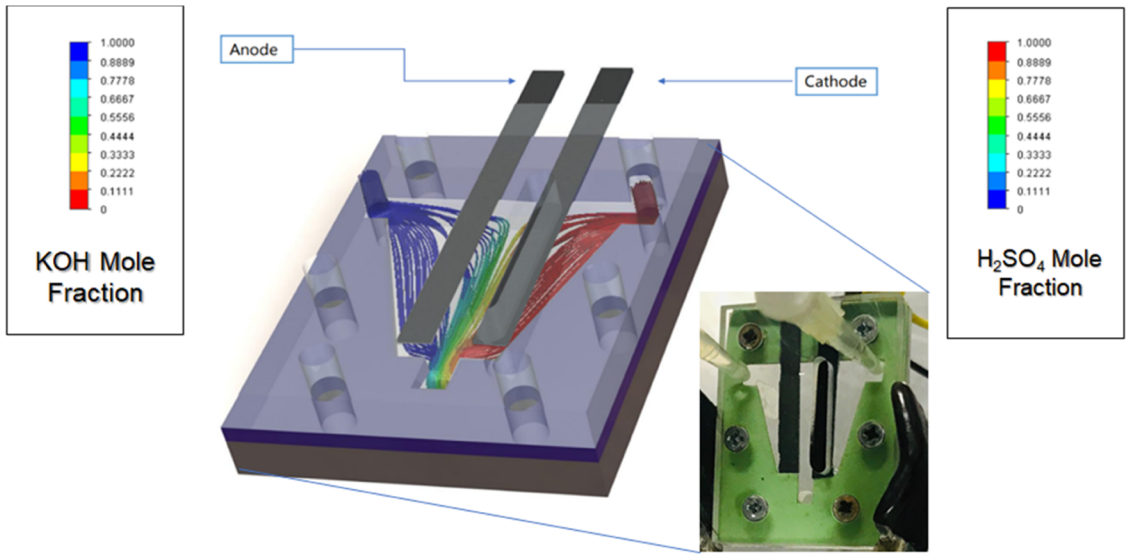

Figure 8. Distribution of the electrolytes injected in the MFC, acid and alkaline, for the catholyte and anolyte, respectively.

with the Pd-MW electrocatalyst, exhibiting the advantage of using the combination of Pd and Co besides the microwave heating during synthesis. This novel procedure can be compared with other studies previously reported, where other materials that are not aerogels do not reach current densities as high as that of the PdCo-MW aerogel (see Table 1).

Based on the results in the half-cell, PdCo-MW vs Pd-MW aerogels were selected to be compared in the MFC (Figure 7) in order to corroborate the contribution of Co in the electrocatalytic activity of the materials.

In the case of the results obtained with the Pd-MW electrocatalyst, 22 mW cm^{-2} as maximum power density was obtained with an OCV of 0.88 V; meanwhile, when PdCo-MW was used as the anodic electrocatalyst, an increase of 1 order of magnitude in the maximum power density value (120 mW cm^{-2}) and an OCV of 1.59 V were achieved. In addition, maximum current densities of 330 and 80 mA cm^{-2} were achieved with PdCo-MW and Pd-MW, respectively (Figure 7a). It is important to note that the high OCV values are due to the properties of the catalytic material in combinations with the pH gradient in the system (anolyte and catholyte), as has already been reported in some studies.[49−51]

Finally, the electrochemical stability of the synthesized materials was also evaluated in the microfluidic fuel cell for a prolonged period of time (70 h). Figure 7b shows a stable performance for the MFC that uses the PdCo-MW aerogel compared to that of the sole palladium aerogel (Pd-MW), which is maintained along the time. Therefore, the presence of cobalt in the aerogel not only improves the catalytic performance toward the EOR but also clearly improves the material stability by maintaining the excellent performance for more than 70 h.

Figure 8 presents a schematic representation of the homogeneous distribution of the electrolytes, which have different characteristics such as pH and density, used in the microfluidic device. This profile was obtained by simulation experiments using Open FOAM CFD simulation software, where at 200 μL min^{-1} flux rate, the interface formation under the laminar flux is guaranteed.

Furthermore, Figure 5d,e shows a comparative XPS study for the sample of PdCo-MW before and after current−time stability tests of the electrocatalyst for 70 h (Figure 7b), where the oxidation states in Pd 3d are observed, with the peaks in Pd^0 and Pd^{2+}, Co 2p, with the peaks of Co^{2+} and Co^{3+}. It can be appreciated that no change in the average width of the peak

https://doi.org/10.1021/acsaem.3c00173
ACS Appl. Energy Mater. 2023, 6, 6410−6418

Table 2. Comparison of MFC Performance Using Ethanol as Fuel

Anode	Cathode	Electrode Area (cm^2)	Fuel	Electrolyte	Flow Rate (μL/min)	OCV (V)	Power Density (mW cm^{-2})	Maximum Current Density (mA cm^{-2})	Reference
Pd−Ag/MWCNT (2 mg)	Pt/C (30 wt %) (2 mg)	0.09	3 M ethanol; air-breathing	1 M KOH	200	0.95	14.5	34	42
Pt−Ru (1:1) (4 mg cm^{-2})	Ag−Pt/graphene (0.04 mg cm^{-2})	0.015	2 M ethanol; air-breathing	0.5 M KOH	2.8	0.75	10	54	43
PtRu/C-Sb	Pt-C (60 wt %) (5 mg)	0.1963	1 M ethanol	0.1 M H_2SO_4	200	0.74	23.27	68.06	44
Pd/C			1.5 M ethanol; air-breathing	0.5 M H_2SO_4 and 0.3 M KOH		1.03	99.66	400	45
Pd−NiO/C (1 mg)	Pt/C (1 mg)	0.015	1.5 M ethanol; air-breathing	0.5 M H_2SO_4 and 0.3 M KOH	2.5	1.11	108	242	46
$Pt_{80}Sn_{10}Ni_{10}$/C	C (2 mg cm^{-2})	0.3	1 M ethanol; 0.1 M sodium percarbonate	0.5 M H_2SO_4		0.71	37.77	226.61	47
Pt−Sn−Ru/C (7:1:2) (2 mg cm^{-2})	Pt/C (2 mg cm^{-2})	0.3	1 M ethanol; 0.1 M sodium	0.5 M H_2SO_4	300	0.63	36	230.2	48
PdCo-MW	Pt/C (2 mg cm^{-2})	0.02	1 M ethanol	1 M KOH	200	1.59	120	330	this work
Pd-MW	Pt/C (2 mg cm^{-2})	0.02	1 M ethanol	1 M KOH	200	0.88	22	80	this work

for both elements occurred, which indicates that there was no oxidation state change of the material. However, it is observed that the intensity of the high peak decreases; this behavior is attributed to the fact that the material remains stable in the polarization tests of MFC.

Finally, for comparative purposes with the aerogels presented in this work, Table 2 presents the MFC performance previously published using several electrocatalysts (not aerogels) in the presence of ethanol as fuel.

4. CONCLUSIONS

The PdCo-MW aerogel was successfully synthesized by an innovative method based on microwave heating. The use of microwaves significantly increases the specific surface area and the presence of Pd^0, which are relevant for further electrochemical reactions. Furthermore, the combination of cobalt with palladium not only increases the specific surface area but also leads to a significant increase in mesoporosity (also called as feeder pores). On the other hand, the interplanar spacing of Pd(111) measured by HR-TEM shows an increase for the PdCo aerogels compared to that of the Pd aerogel alone and a slight increase in the case of using microwave heating during the synthesis, indicating the presence of Pd−Co metallic alloys and a beneficial effect of using microwaves.

All of these physicochemical properties of the PdCo-MW aerogel offer a great advantage for electrochemical applications, especially for the ethanol oxidation reaction, even in microfluidic fuel cells, where the current density reached a value of 330 mA cm^2 (more than 3 times that of the palladium aerogel), besides a much greater stability over time. Moreover, this type of electrocatalytic material with high surface area, active sites, and stability could be widely used for oxidation reactions of several fuels and applied in electrochemical energy systems.

■ ASSOCIATED CONTENT

Supporting Information

The Supporting Information is available free of charge at https://pubs.acs.org/doi/10.1021/acsaem.3c00173.

Additional experimental details of the aerogel synthesis procedure, including photographs of the experimental setup (PDF)

■ AUTHOR INFORMATION

Corresponding Authors

J. Ledesma-García − *División de Investigación y Posgrado, Facultad de Ingeniería, Universidad Autónoma de Querétaro, 76010 Santiago de Querétaro, Mexico;* orcid.org/0000-0002-0677-4280; Email: janet.ledesma@uaq.mx

A. Arenillas − *Instituto de Ciencia y Tecnología del Carbono, INCAR-CSIC, 33011 Oviedo, Spain*; Email: aapuente@incar.csic.es

Authors

A. Martínez-Lázaro − *División de Investigación y Posgrado, Facultad de Ingeniería, Universidad Autónoma de Querétaro, 76010 Santiago de Querétaro, Mexico*

A. P. Mendoza-Camargo − *División de Investigación y Posgrado, Facultad de Ingeniería, Universidad Autónoma de Querétaro, 76010 Santiago de Querétaro, Mexico*

M. H. Rodriguez-Barajas − *División de Investigación y Posgrado, Facultad de Ingeniería, Universidad Autónoma de Querétaro, 76010 Santiago de Querétaro, Mexico*

F. I. Espinosa-Lagunes − *Centro de Investigación y Desarrollo Tecnológico en Electroquímica, 76703 Santiago de Querétaro, Mexico*

Y. Salazar-Lara − *Centro de Investigación y Desarrollo Tecnológico en Electroquímica, 76703 Santiago de Querétaro, Mexico*

A. Herrera-Gomez − *Centro de Investigación y de Estudios Avanzados, 76230 Santiago de Querétaro, Mexico*

O. Cortazar-Martínez − *Centro de Investigación y de Estudios Avanzados, 76230 Santiago de Querétaro, Mexico*

N. Rey-Raap − *Instituto de Ciencia y Tecnología del Carbono, INCAR-CSIC, 33011 Oviedo, Spain*

L. G. Arriaga − *Centro de Investigación y Desarrollo Tecnológico en Electroquímica, 76703 Santiago de Querétaro, Mexico;* orcid.org/0000-0001-5052-2294

Complete contact information is available at:

https://pubs.acs.org/10.1021/acsaem.3c00173

Notes

The authors declare no competing financial interest.

■ ACKNOWLEDGMENTS

The authors thank Consejo Nacional de Humanidades, Ciencias y Tecnologías (CONAHCYT) for funding through the Ciencia de Frontera 2020-845132.

■ REFERENCES

(1) Safdar, M.; Jänis, J.; Sánchez, S. Microfluidic fuel cells for energy generation. *Lab Chip* **2016**, *16*, 2754−2758.
(2) Liu, C.; Sun, C.; Gao, Y.; Lan, W.; Chen, S. Improving the Electrochemical Properties of Carbon Paper as Cathodes for Microfluidic Fuel Cells by the Electrochemical Activation in Different Solutions. *ACS Omega* **2021**, *6*, 19153−19161.
(3) Pihosh, Y.; Uemura, J.; Turkevych, I.; Mawatari, K.; Kazoe, Y.; Smirnova, A.; Kitamori, T. From Extended Nanofluidics to an Autonomous Solar-Light-Driven Micro Fuel-Cell Device. *Angew. Chem., Int. Ed.* **2017**, *56*, 8130−8133.
(4) Santoro, C.; Kodali, M.; Herrera, S.; Serov, A.; Leropoulos, I.; Atanassov, P. Power generation in microbial fuel cells using platinum group metal-free cathode catalyst: Effect of the catalyst loading on performance and costs. *J. Power Sources* **2018**, *378*, 169−175.
(5) Oezaslan, M.; Liu, W.; Nachtegaal, M.; Frenkel, A. I.; Rutkowski, B.; Werheid, M.; Herrmann, A. K.; Laugier-Bonnaud, C.; Yilmaz, H. C.; Gaponik, N.; Czyrska-Filemonowicz, A.; Eychmüller, A.; Schmid, T. J. Homogeneity and elemental distribution in self-assembled bimetallic Pd-Pt aerogels prepared by a spontaneous one-step gelation process. *Phys. Chem. Chem. Phys.* **2016**, *18*, 20640−20650.
(6) Wen, D.; Liu, W.; Haubold, D.; Zhu, C.; Oschatz, M.; Holzschuh, M.; Wolf, A.; Simon, F.; Kaskel, S.; Eychmüller, A. Gold Aerogels: Three-Dimensional Assembly of Nanoparticles and Their Use as Electrocatalytic Interfaces. *ACS Nano* **2016**, *10*, 2559−2567.
(7) Wang, J.; Chen, F.; Jin, Y.; Guo, L.; Gong, X.; Wang, X.; Johnston, R. L. In situ high-potential-driven surface restructuring of ternary AgPd-Ptdilute aerogels with record-high performance improvement for formate oxidation electrocatalysis. *Nanoscale* **2019**, *11*, 14174−14185.
(8) Henning, S.; Ishikawa, H.; Kühn, L.; Herranz, J.; Müller, E.; Eychmüller, A.; Schmidt, T. J. Unsupported Pt-Ni Aerogels with Enhanced High Current Performance and Durability in Fuel Cell Cathodes. *Angew. Chem., Int. Ed.* **2017**, *56*, 10707−10710.
(9) Liu, W.; Herrmann, A. K.; Bigall, N. C.; Rodriguez, P.; Wen, D.; Oezaslan, M.; Schmidt, T. J.; Gaponik, N.; Eychmüller, A. Noble metal aerogels-synthesis, characterization, and application as electrocatalysts. *Acc. Chem. Res.* **2015**, *48*, 154−162.
(10) Gao, F.; Zhang, Y.; Ren, F.; Shiraishi, Y.; Du, Y. Universal Surfactant-Free Strategy for Self-Standing 3D Tremella-Like Pd−M (M = Ag, Pb, and Au) Nanosheets for Superior Alcohols Electrocatalysis. *Adv. Funct. Mater.* **2020**, *30*, No. 2000255.
(11) Gao, F.; Zhang, Y.; Wu, Z.; You, H.; Du, Y. Universal strategies to multi-dimensional noble-metal-based catalysts for electrocatalysis. *Coord. Chem. Rev.* **2021**, *436*, No. 213825.
(12) Zhao, Q.; Chu, C.; Xiao, X.; Chen, B. Selectively coupled small Pd nanoparticles on sp2-hybridized domain of graphene-based aerogel with enhanced catalytic activity and stability. *Sci. Total Environ* **2021**, *771*, No. 145396.
(13) Zhou, Q.; Su, Z.; Tang, Y.; Ai, L.; Fu, G.; Wu, Z.; Sun, D.; Tang, Y. Pt-Like Oxygen Reduction Activity Induced by Cost-Effective MnFeO 2 /N-Carbon. *Chem. − Eur. J.* **2019**, *25*, 6226−6232.
(14) Lee, J. Y.; Kwak, D. H.; Lee, Y. W.; Lee, S.; Park, K.W. Synthesis of cubic PtPd alloy nanoparticles as anode electrocatalysts for methanol and formic acid oxidation reactions. *Phys. Chem. Chem. Phys.* **2015**, *17*, 8642−8648.
(15) Zhu, C.; Liu, D.; Chen, Z.; Li, L.; You, T. Superior catalytic activity of Pt/carbon nanohorns nanocomposites toward methanol and formic acid oxidation reactions. *J. Colloid Interface Sci.* **2018**, *511*, 77−83.
(16) Han, A.; Zhang, Z.; Yang, J.; Wang, D.; Li, Y. Carbon-Supported Single-Atom Catalysts for Formic Acid Oxidation and Oxygen Reduction Reactions. *Small* **2021**, *17*, No. 2004500.
(17) Yu, X.; Dos Santos, E. C.; White, J.; Salazar-Alvarez, G.; Pettersson, L. G. M.; Cornell, A.; Johnsson, M. Electrocatalytic Glycerol Oxidation with Concurrent Hydrogen Evolution Utilizing an Efficient MoOx/Pt Catalyst. *Small* **2021**, *17*, No. 2104288.
(18) Wu, X.; Fang, G.; Tong, Y.; Jiang, D.; Liang, Z.; Leng, W.; Liu, L.; Tu, P.; Wang, H.; Ni, J.; Li, X. Catalytic Upgrading of Ethanol to n-Butanol: Progress in Catalyst Development. *ChemSusChem* **2018**, *11*, 71−85.
(19) Feng, Y.; Long, S.; Tang, X.; Sun, Y.; Luque, R.; Zeng, X.; Lin, L. Earth-abundant 3d-transition-metal catalysts for lignocellulosic biomass conversion. *Chem. Soc. Rev.* **2021**, *50*, 6042−6093.
(20) Hu, K.; Ohto, T.; Nagata, Y.; Wakisaka, M.; Aoki, Y.; Fujita, J.; Ito, Y. Catalytic activity of graphene-covered non-noble metals governed by proton penetration in electrochemical hydrogen evolution reaction. *Nat. Commun.* **2021**, *12*, No. 203.
(21) Habibullah, G.; Viktorova, J.; Ruml, T. Current Sstrategies for noble metal nanoparticle synthesis. *Nanoscale Res. Lett.* **2021**, *16*, 47.
(22) Gurrola, M. P.; Ortiz-Ortega, E.; Farias-Zuñiga, C.; Chávez-Ramírez, A. U.; Ledesma-García, J.; Arriaga, L. G. Evaluation and coupling of a membraneless nanofluidic device for low-power applications. *J. Power Sources* **2016**, *307*, 244−250.
(23) Choi, S.; Oh, M. Well-arranged and confined incorporation of PdCo nanoparticles within a hollow and porous metal−organic framework for superior catalytic activity. *Angew. Chem., Int. Ed.* **2019**, *58*, 866−871.
(24) Zhao, C.; Yan, X.; Wang, G.; Jin, Y.; et al. PdCo bimetallic nano-electrocatalyst as effective air-cathode for aqueous metal-air batteries. *Int. J. Hydrogen Energy* **2018**, *43*, 5001−5011.
(25) Zhu, X.; Zhang, B.; Ye, D. D.; Li, J.; Liao, Q. Air-breathing direct formic acid microfluidic fuel cell with an array of cylinder anodes. *J. Power Sources* **2014**, *247*, 346−353.
(26) Sen, B.; Acidereli, H.; Karaman, N.; Sen, F. Monodisperse palladium−cobalt alloy nanocatalyst supported on activated carbon (AC) as highly effective catalyst for the DMAB dehydrocoupling. *Sci. Rep.* **2020**, *10*, No. 11755.
(27) Anicai, L.; Costovici, S.; Cojocaru, A.; Manea, A.; Visan, T. Electrodeposition of Co and CoMo alloys coatings using choline chloride based ionic liquids − evaluation of corrosion behaviour. *Trans. IMF* **2015**, *93*, 302−312.
(28) Eftekhari, A.; Fang, B. Electrochemical hydrogen storage: opportunities for fuel storage, batteries, fuel cells, and supercapacitors. *Int. J. Hydrogen Energy* **2017**, *42*, 25143−25165.
(29) Oh, H. J.; Dao, V. D.; Choi, H. S. Cost-effective CoPd alloy/reduced graphene oxide counter electrodes as a new avenue for high-efficiency liquid junction photovoltaic devices. *J. Alloys Compd.* **2017**, *705*, 610−617.
(30) Xu, G. R.; Han, C. C.; Zhu, Y. Y.; Zeng, J. H.; Jiang, J. X.; Chen, Y. PdCo Alloy Nanonetworks−Polyallylamine Inorganic−Organic Nanohybrids toward the Oxygen Reduction Reaction. *Adv. Mater. Interfaces* **2018**, *5*, No. 1701322.
(31) Zhang, J. W.; Zhang, B.; Zhang, X. Enhanced catalytic activity of ternary NiCoPd nanocatalyst dispersed on carbon nanotubes toward methanol oxidation reaction in alkaline media. *J. Solid State Electrochem.* **2017**, *21*, 447−453.
(32) Cabrera-German, D.; Gomez, G.; Herrera, A. Accurate peak fitting and subsequent quantitative composition analysis of the spectrum of Co 2p obtained with Al Kα radiation: I: cobalt spinel. *Surf. Interface Anal.* **2016**, *48*, 252−256.
(33) Chakraborty, A.; Kunnikuruvan, S.; Kumar, S.; Markovsky, B.; Aurbach, D.; Dixit, M.; Major, D. T. Layered cathode materials for lithium-ion batteries: review of computational studies on $LiNi_{1-x-y}$

Co_x Mn_y O_2 and $LiNi_{1-x-y}$ $Co_xAl_yO_2$. *Chem. Mater.* **2020**, *32*, 915−952.
(34) Prieto, P.; Marco, J. F.; Serrano, A.; Manso, M.; De la Figuera, J. Highly oriented (111) CoO and Co_3O_4 thin films grown by ion beam sputtering. *J. Alloys Compd.* **2019**, *810*, No. 151912.
(35) Melo, R. S.; Silva, F. C.; Moura, K. R. M.; De Menezes, A. S.; Sinfrônio, F. S. M. Magnetic ferrites synthesised using the microwave-hydrothermal method. *J. Magn. Magn. Mater.* **2015**, *381*, 109−115.
(36) Asim, M.; Saba, N.; Sapuan, S. M.; Nasir, I. M.Potential of Natural Fiber/biomass Filler-Reinforced Polymer Composites in Aerospace Applications. In *Sustainable Composites for Aerospace Applications*; Woodhead Publishing, 2018; pp 253−268.
(37) Guo, F.; Li, Y.; Fan, B.; Liu, Y.; Lu, L.; Lei, Y. Carbon- and binder-free core−shell nanowire arrays for efficient ethanol electro-oxidation in alkaline medium. *ACS Appl. Mater. Interfaces* **2018**, *10*, 4705−4714.
(38) Park, C. E.; Lee, H.; Senthil, R. A.; Jeong, G. H.; Choi, M. Y. Bimetallic nickel-palladium nanoparticles with low Ni content and their enhanced ethanol oxidation performance: using a pulsed laser as modification machinery. *Fuel* **2022**, *321*, No. 124108.
(39) Ruiz-Montoya, J. G.; Nunes, L.M.S.; Baena, A. M.; Tremiliosi, G.; Morales, J. C. Effect of palladium on gold in core-shell catalyst for electrooxidation of ethanol in alkaline medium. *Int. J. Hydrogen Energy* **2021**, *46*, 23670−23681.
(40) Yasmin, S.; Roy, N.; Kabir, M. H.; Jeon, S. Nitrogen-functionalized carbon nanotube based palladium nanoparticles as an efficient catalyst for oxygen reduction and ethanol oxidation reaction. *Appl. Surf. Sci. Adv.* **2022**, *9*, No. 100235.
(41) Zhiani, M.; Rostami, H.; Majidi, M.; Karami, K. Bis (dibenzylidene acetone) palladium (0) catalyst for glycerol oxidation in half cell and in alkaline direct glycerol fuel cell. *Int. J. Hydrogen Energy* **2013**, *38*, 5435−5441.
(42) Armenta-González, A.; Carrera, R.; Moreno, A.; Álvarez, L.; Ledesma, J.; Cuevas, F. M.; Arriaga, L. G. An improved ethanol microfluidic fuel cell based on a PdAg/MWCNT catalyst synthesized by the reverse micelles method. *Fuel* **2016**, *167*, 240−247.
(43) Estrada-Solís, M.; Abrego-Martínez, J. C.; Moreno, A.; Arriaga, L. G.; Sun, S.; Cuevas, F. M.; Mohamedi, M. Use of a bilayer platinum-silver cathode to selectively perform the oxygen reduction reaction in a high concentration mixed-reactant microfluidic direct ethanol fuel cell. *Int. J. Hydrogen Energy* **2019**, *44*, 18372−18381.
(44) Figueiredo, M. C.; Sorsa, O.; Arán, R. M.; Doan, N.; Feliu, J. M.; Kallio, T. Trimetallic catalyst based on PtRu modified by irreversible adsorption of Sb for direct ethanol fuel cells. *J. Catal.* **2015**, *329*, 69−77.
(45) López-Rico, C. A.; Galindo de la Rosa, J.; Álvarez, L.; Ledesma, J.; Guerra, M.; Arriaga, L. G.; Arjona, N. Direct Ethanol Membraneless Nanofluidic Fuel Cell With High Performance. *ChemistrySelect* **2016**, *1*, 3054−3062.
(46) López-Rico, C.; Galindo de la Rosa, J.; Ortiz, E.; Álvarez, L.; Ledesma, J.; Guerra, M.; Arriaga, L. G.; Arjona, N. High performance of ethanol co-laminar flow fuel cells based on acrylic, paper and Pd-NiO as anodic catalyst. *Electrochim. Acta* **2016**, *207*, 164−176.
(47) Ponmani, K.; Kiruthika, S.; Muthukumaran, B. Investigation of nanometals (Ni and Sn) in platinum-based ternary electrocatalysts for ethanol electro-oxidation in membraneless fuel cells. *J. Electrochem. Sci. Technol.* **2015**, *6*, 95−105.
(48) Ponmani, K.; Nayeemunisa, S. M.; Kiruthika, S.; Muthukumaran, B. Electrochemical characterization of platinum-based anode catalysts for membraneless fuel cells. *Ionics* **2016**, *22*, 377−387.
(49) Arun, A.; Gowdhamamoorthi, M.; Kiruthika, S.; Muthukumaran, B. Analysis of Membraneless Methanol Fuel Cell Using Percarbonate as an Oxidant. *J. Electrochem. Soc.* **2014**, *161*, F311−F317.
(50) Chandra, S.; Lal, S.; Janardhanan, V.; Chandra Sahu, K.; Deepa, M. Ethanol Based Fuel Cell on Paper Support. *J. Power Sources* **2018**, *396*, 725−733.
(51) Priya, M.; Arun, A.; Elumalai, M.; Kiruthika, S.; Muthukumaran, B. A Development of Ethanol / Percarbonate Membraneless Fuel Cell. *Adv. Phys. Chem.* **2014**, *2014*, No. 862691.

https://doi.org/10.1021/acsaem.3c00173
ACS Appl. Energy Mater. 2023, 6, 6410−6418